

## HATS-5b: A TRANSITING HOT-SATURN FROM THE HATSOUTH SURVEY <sup>†</sup>

G. ZHOU<sup>1</sup>, D. BAYLISS<sup>1</sup>, K. PENEV<sup>2,3</sup>, G. Á. BAKOS<sup>2,3,\*,\*\*</sup>, J. D. HARTMAN<sup>2,3</sup>, A. JORDÁN<sup>4</sup>, L. MANCINI<sup>5</sup>, M. MOHLER<sup>5</sup>, Z. CSUBRY<sup>2,3</sup>, S. CICERI<sup>5</sup>, R. BRAHM<sup>4</sup>, M. RABUS<sup>4</sup>, L. BUCHHAVE<sup>6</sup>, T. HENNING<sup>5</sup>, V. SUC<sup>4</sup>, N. ESPINOZA<sup>4</sup>, B. BÉKY<sup>3</sup>, R. W. NOYES<sup>3</sup>, B. SCHMIDT<sup>1</sup>, R. P. BUTLER<sup>7</sup>, S. SHECTMAN<sup>8</sup>, I. THOMPSON<sup>8</sup>, J. CRANE<sup>8</sup>, B. SATO<sup>9</sup>, B. CSÁK<sup>5</sup>, J. LÁZÁR<sup>10</sup>, I. PAPP<sup>10</sup>, P. SÁRI<sup>10</sup>, N. NIKOLOV<sup>11,5</sup>

*Draft version 04 January 9, 2014*

### ABSTRACT

We report the discovery of HATS-5b, a transiting hot-Saturn orbiting a G type star, by the HATSouth survey. HATS-5b has a mass of  $M_p \approx 0.24 M_J$ , radius of  $R_p \approx 0.91 R_J$ , and transits its host star with a period of  $P \approx 4.7634$  d. The radius of HATS-5b is consistent with both theoretical and empirical models. The host star has a *V* band magnitude of 12.6, mass of  $0.94 M_\odot$ , and radius of  $0.87 R_\odot$ . The relatively high scale height of HATS-5b, and the bright, photometrically quiet host star, make this planet a favourable target for future transmission spectroscopy follow-up observations. We reexamine the correlations in radius, equilibrium temperature, and metallicity of the close-in gas-giants, and find hot Jupiter-mass planets to exhibit the strongest dependence between radius and equilibrium temperature. We find no significant dependence in radius and metallicity for the close-in gas-giant population.

*Subject headings:* planetary systems — stars: individual (HATS-5, GSC 5897-00933) techniques: spectroscopic, photometric

### 1. INTRODUCTION

Transiting planets are the best characterised planets outside of our solar system. The transit geometry allow us to measure the mass, radius, and characterise the atmosphere (e.g. Charbonneau et al. 2002; Deming et al. 2005) and dynamics (e.g. Queloz et al. 2000) of individual planets. As a result the of discoveries from wide-field ground and space-based photometric surveys (e.g. Bakos et al. 2004; Pollacco et al. 2006;

Borucki et al. 2010; Bakos et al. 2013), statistical studies have revealed that close-in gas-giants are rare (e.g. Howard et al. 2012; Fressin et al. 2013), have relatively dark albedos (e.g. Cowan & Agol 2011), and are found preferentially around metal-rich stars (e.g. Santos et al. 2004; Buchhave et al. 2012).

Previous studies have also explored effect of irradiation and composition in inflating the radius of gas giants (e.g. Guillot et al. 2006; Enoch et al. 2011; Béky et al. 2011; Enoch et al. 2012). In particular, Enoch et al. (2011, 2012) found that the radius of Saturn-mass planets are more dependent on metallicity than Jupiter-mass planets, revealing a mass dependence to the inflation mechanisms.

Intensive ground-based follow-up observations are extremely important for the characterisation of transiting gas-giants. Due to the mass degeneracy in the gas-giant regime, Saturns, Jupiters, and brown dwarfs cannot be distinguished from discovery transit photometry alone. The mass degeneracy is a major limitation against using the *Kepler* candidate sample to study mass-dependent statistics of close-in gas-giant planets. The rarity of close-in gas giants, and the relative difficulty of characterising hot-Saturns compared to hot-Jupiters, leaves the hot-Saturn regime still poorly explored. Of the 299 confirmed transiting planets<sup>15</sup>, only 23 have masses in range of Saturn ( $0.1 < M_p < 0.5 M_J$ ) and are found in close-in orbits ( $P < 10$  days). As a result, our statistical understanding of the hot-Saturn population is relatively less mature.

In this study, we report the discovery of the transiting hot-Saturn HATS-5b by the HATSouth survey. The HATSouth discovery, photometric and spectroscopic follow-up observations are detailed in Section 2. Analyses of the results, including derivation of host star parameters, global modelling of the data, blend analyses,

<sup>1</sup> Research School of Astronomy and Astrophysics, Australian National University, Canberra, ACT 2611, Australia; email: george.zhou@anu.edu.au

<sup>2</sup> Department of Astrophysical Sciences, Princeton University, NJ 08544, USA

<sup>3</sup> Harvard-Smithsonian Center for Astrophysics, Cambridge, MA, USA

\* Alfred P. Sloan Research Fellow

\*\* Packard Fellow

<sup>4</sup> Departamento de Astronomía y Astrofísica, Pontificia Universidad Católica de Chile, Av. Vicuña Mackenna 4860, 7820436 Macul, Santiago, Chile

<sup>5</sup> Max Planck Institute for Astronomy, Heidelberg, Germany

<sup>6</sup> Niels Bohr Institute, Copenhagen University, Denmark

<sup>7</sup> Department of Terrestrial Magnetism, Carnegie Institution of Washington, 5241 Broad Branch Road NW, Washington, DC 20015-1305, USA

<sup>8</sup> The Observatories of the Carnegie Institution of Washington, 813 Santa Barbara Street, Pasadena, CA 91101, USA

<sup>9</sup> Department of Earth and Planetary Sciences, Tokyo Institute of Technology, 2-12-1 Ookayama, Meguro-ku, Tokyo 152-8551

<sup>10</sup> Hungarian Astronomical Association, Budapest, Hungary

<sup>11</sup> Astrophysics Group, School of Physics, University of Exeter, Stocker Road, Exeter EX4 4QL, UK

<sup>†</sup> The HATSouth network is operated by a collaboration consisting of Princeton University (PU), the Max Planck Institute für Astronomie (MPIA), and the Australian National University (ANU). The station at Las Campanas Observatory (LCO) of the Carnegie Institute is operated by PU in conjunction with collaborators at the Pontificia Universidad Católica de Chile (PUC), the station at the High Energy Spectroscopic Survey (HESS) site is operated in conjunction with MPIA, and the station at Siding Spring Observatory (SSO) is operated jointly with ANU.

and constraints on the wavelength-radius relationship, are described in Section 3. In Section 4, we revisit some of the statistical trends for the close-in gas-giant population, and discuss HATS-5b in the context of the known hot-Saturns and hot-Jupiters.

## 2. OBSERVATIONS

### 2.1. Photometric detection

The transit signal around HATS-5 was first detected from photometric observations by the HATSouth survey (Bakos et al. 2013). HATSouth is a network of identical, fully-robotic telescopes located at three sites spread around the Southern Hemisphere, allowing continuous coverage of the surveyed fields. Altogether 8066 observations of HATS-5 were obtained by the HATSouth units HS-1 in Chile, HS-3 in Namibia, and HS-5 in Australia from September 2009 to December 2010. Each unit consists of four 0.18 m f/2.8 Takahasi astrographs and Apogee 4K×4K U16M Alta CCD cameras. Each telescope has a field of view of  $4^\circ \times 4^\circ$ , with a pixel scale of  $3.7''\text{pixel}^{-1}$ . The observations are performed with 4 minute exposures through the Sloan  $r'$  filter.

Discussions of the HATSouth photometric reduction and candidate identification process can be found in detail in Bakos et al. (2013) and Penev et al. (2013). Aperture photometry was performed and detrended using External Parameter Decorrelation (EPD, Bakos et al. 2007) and Trend Filtering Algorithm (TFA, Kovács et al. 2005). Transit signals were identified using the Box-fitting Least Squares analysis (BLS, Kovács et al. 2002). Table 1 summarises the photometric observations for HATS-5. The HATSouth discovery light curve is plotted in Figure 1.

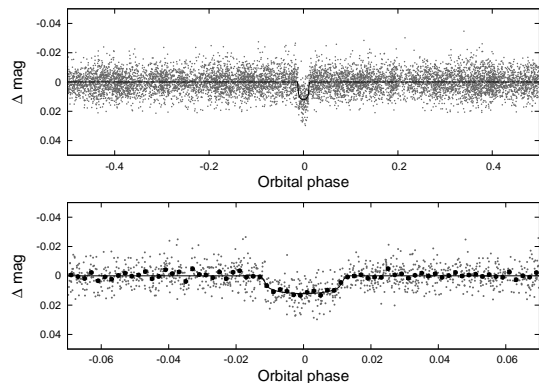


FIG. 1.— HATSouth  $r'$ -band discovery light curve, unbinned, and folded with a period of  $P = 4.7633872$  days, as per the analysis in Section 3. Solid line shows the best fit transit model. The lower panel shows the transit region of the light curve. Dark filled points represent the light curve binned at 0.002 in phase.

### 2.2. Spectroscopy

Spectroscopic confirmation of HATS-5b consisted of separate reconnaissance observations to exclude most stellar binary false-positive scenarios that can mimic the transit signal of an exoplanet. High resolution, high signal-to-noise measurements of the radial velocity (RV) variation for HATS-5 were then obtained to confirm the planetary status of HATS-5b. The spectroscopic follow-up observations are presented in Table 2.

Low resolution reconnaissance observations were performed using the Wide Field Spectrograph (WiFeS, Dopita et al. 2007) on the ANU 2.3 m telescope at Siding Spring Observatory, Australia. A flux calibrated spectrum was obtained at  $R \equiv \lambda/\Delta\lambda = 3000$  to provide an initial spectral classification of HATS-5 as an G-dwarf with  $T_{\text{eff}} = 5300$  K,  $\log g = 4.5$ , and  $[\text{Fe}/\text{H}] = 0$ . These stellar parameters are later refined by higher resolution observations (Section 3). Multi-epoch observations at  $R = 7000$  confirmed the candidate did not exhibit  $> 1 \text{ km s}^{-1}$  RV variations. Such velocity variations are indicative of eclipsing stellar binaries, which have so far made up  $\sim 30\%$  of HATSouth candidates. Details of the WiFeS follow-up procedure and stellar binary identification process can be found in Bayliss et al. (2013) and Zhou et al. (2013). Candidates that pass the WiFeS vetting process are passed on to higher resolution observations.

HATS-5 received nine high resolution ( $R = 60000$ ) reconnaissance RV observations with the CORALIE spectrograph on the Swiss Leonard Euler 1.2 m telescope at La Silla Observatory, Chile, and fourteen  $R = 48000$  observations with the FEROS spectrograph on the ESO/MPG 2.2 m telescope at La Silla. Detailed descriptions of the acquisition, reduction, and analyses of the CORALIE and FEROS observations can be found in the previous HATSouth discovery papers (Penev et al. 2013; Mohler-Fischer et al. 2013). Velocities from these observations allowed us to constrain the RV orbit semi-amplitude to be  $< 45 \text{ m s}^{-1}$ .

The upper limit RV constraints from CORALIE, FEROS, and WiFeS indicated that HATS-5b is a low density gas-giant. High signal-to-noise, high resolution observations were required to determine the RV orbit of the system. Velocities of HATS-5 were obtained Planet Finding Spectrograph (PFS) on the 6.5 m Magellan Baade telescope at Las Campanas Observatory, Chile, and the High Dispersion Spectrograph (HDS) on the 8.2 m Subaru telescope at Maunakea Kea Observatory, Hawaii. The PFS and HDS velocities and bisector spans are presented in Table 3, the RV orbit is plotted in Figure 2.

The Subaru/HDS (Noguchi et al. 2002) observations were carried out on the nights of 19–22 Sep 2012 UT. Observations were made using an  $\text{I}_2$  cell on four of the nights (Kambe et al. 2002), and without the  $\text{I}_2$  cell on one of the nights. We used the KV370 filter, the  $0''.6 \times 2''.0$  slit, and the StdI2b setup, yielding spectra with a resolution of  $R = 60000$  and wavelength coverage of 3500–6200 Å. On each night we obtained three consecutive observations yielding a total S/N per resolution element of  $\sim 100$ . The observations are split into three to reduce the impact of cosmic ray contamination and changes in the barycentric velocity correction over the course of an exposure. The  $\text{I}_2$ -free observations were used to create a template spectrum needed to measure precise relative RV values from the observations made with the  $\text{I}_2$  cell. The individual spectra were reduced to RV measurements using the procedure of Sato et al. (2002, 2012), which in turn is based on the method of Butler et al. (1996). Additionally we measured spectral line bisectors following Bakos et al. (2007) for each observation. The root-mean-squared (RMS) scatter of the HDS velocities from the

TABLE 1  
SUMMARY OF PHOTOMETRIC OBSERVATIONS

Facility	Date(s)	Number of Images <sup>a</sup>	Cadence (s) <sup>b</sup>	Filter
HS-1 (Chile)	2009 Nov–2010 Dec	3953	290	Sloan <i>r</i>
HS-3 (Namibia)	2009 Sep–2010 Dec	3241	288	Sloan <i>r</i>
HS-5 (Australia)	2010 Sep–2010 Dec	900	287	Sloan <i>r</i>
ESO/MPG 2.2 m/GROND	2012 Oct 10	178	93	Sloan <i>g</i>
ESO/MPG 2.2 m/GROND	2012 Oct 10	107	93	Sloan <i>r</i>
ESO/MPG 2.2 m/GROND	2012 Oct 10	214	93	Sloan <i>i</i>
ESO/MPG 2.2 m/GROND	2012 Oct 10	211	93	Sloan <i>z</i>
ESO/MPG 2.2 m/GROND	2012 Dec 11	159	144	Sloan <i>g</i>
ESO/MPG 2.2 m/GROND	2012 Dec 11	160	144	Sloan <i>r</i>
ESO/MPG 2.2 m/GROND	2012 Dec 11	162	144	Sloan <i>i</i>
ESO/MPG 2.2 m/GROND	2012 Dec 11	162	144	Sloan <i>z</i>

<sup>a</sup> Outlying exposures have been discarded.

<sup>b</sup> Mode time difference between points in the light curve. Uniform sampling was not possible due to visibility, weather, pauses.

best fit Keplerian curve is  $4.8 \text{ ms}^{-1}$ .

HATS-5 was also observed with the Carnegie Planet Finder Spectrograph (PFS, Crane et al. 2010) on Magellan II at Las Campanas Observatory, Chile on the UT nights of 2012 December 28–31, 2013 February 21, and 2013 February 4. We obtained one iodine-free spectrum, and all other spectra were taken using the iodine cell and a slit-width of  $0.5''$ . To increase the signal-to-noise of each spectrum we read-out with  $2 \times 2$  binning and in slow readout mode. Consecutive pairs of 20 min exposures were taken on each night. The RV for each spectrum was determined using the spectral synthesis technique detailed in Butler et al. (1996). The (RMS) scatter of the PFS velocities from the best fit Keplerian curve is  $3.8 \text{ ms}^{-1}$ .

### 2.3. Photometric follow-up observations

High precision photometric follow-ups of a partial and a full transit of HATS-5b were performed on 2012 October 10 and 2012 December 11, respectively, using GROND on the ESO/MPG 2.2m telescope (Greiner et al. 2008). The GROND imager provides simultaneous photometric monitoring in four optical bands ( $g', r', i', z'$ ) over a  $5.4' \times 5.4'$  field of view at  $0.158'' \text{ pixel}^{-1}$  sampling. Details of the GROND observation strategy, reduction, and photometry procedure can be found in Penev et al. (2013) and Mohler-Fischer et al. (2013). The GROND light curves are presented in Table 4 and plotted in Figure 3.

## 3. ANALYSIS

The stellar parameters for HATS-5 are derived from the PFS iodine-free spectrum using the Stellar Parameter Classification (SPC) process described in Buchhave et al. (2012). The derived values for effective temperature, surface gravity, metallicity, and projected rotational velocity are  $T_{\text{eff}} = 5300 \pm 50 \text{ K}$ ,  $\log g = 4.51 \pm 0.10 \text{ cgs}$ ,  $[\text{Fe}/\text{H}] = 0.19 \pm 0.08 \text{ dex}$ , and  $v \sin i = 0.8 \pm 0.5 \text{ km s}^{-1}$ , respectively. The surface gravity is later confirmed from transit light curve fitting as per Sozzetti et al. (2007). The SPC derived stellar parameters agree with the classifications made by the reconnaissance spectroscopic observations to within 10 K in  $T_{\text{eff}}$ , 0.4 dex in  $\log g$ , and 0.2 dex in  $[\text{Fe}/\text{H}]$ .

To derive the system parameters, we performed a global analysis of the HATSouth discovery light curves,

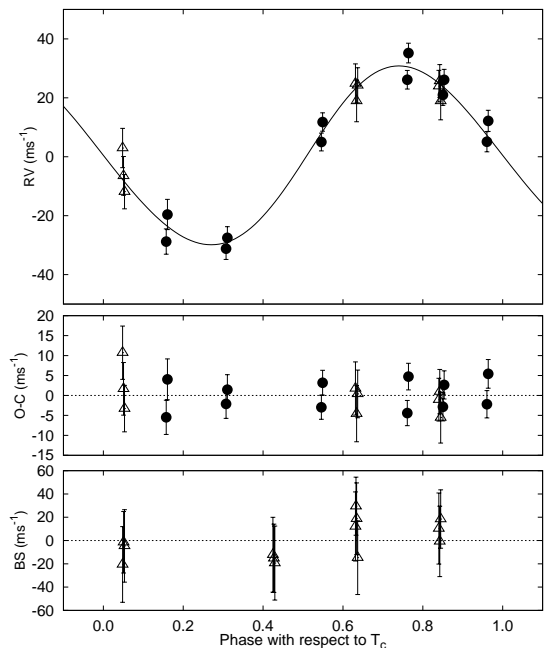


FIG. 2.— *Top panel:* Phased radial velocities (RVs) from Magellan/PFS are plotted as dark filled circles, Subaru/HDS as open triangles. The best fit model is plotted by the solid line. The best fit absolute velocity offset from each instrument has been subtracted from the observations. *Middle panel:* Residuals of the RV measurements from the best fit model. The error bars have been inflated such that the  $\chi^2$  per degree of freedom is unity for each instrument. *Bottom panel:* Bisector spans (BS) are plotted for velocities from Subaru/HDS. Note the different scales for each panel.

follow-up photometry from GROND, and RV orbit measurements from PFS and HDS. The best fit parameters and posteriors are determined using a Markov chain Monte Carlo analysis, the global analysis procedure is fully described in Bakos et al. (2010) and Penev et al. (2013). Following Sozzetti et al. (2007), we use the stellar density from the light curve in the global fit and the spectroscopic stellar parameters,  $T_{\text{eff}}$  and  $[\text{Fe}/\text{H}]$ , to sample from the Yonsei-Yale theoretical isochrones (Yi et al. 2001), deriving the stellar mass and radius for HATS-5. The resulting  $\log g$  from the isochrone sampling matches the spectroscopic  $\log g$  from SPC. The full list of final spectroscopic and derived stellar properties are presented

TABLE 2  
SUMMARY OF SPECTROSCOPIC OBSERVATIONS

Telescope/Instrument	Date Range	Number of Observations	Resolution	Observing Mode
Reconnaissance				
ANU 2.3 m/WiFeS	2012 Aug 4	1	3000	RECON Spec <sup>a</sup>
ANU 2.3 m/WiFeS	2012 Aug 4–6	3	7000	RECON RV <sup>b</sup>
Euler 1.2 m/Coralie	2012 Aug 21–2013 Feb 27	9	60000	ThAr/RECON RV
ESO/MPG 2.2 m/FEROS	2012 Nov 21–2013 Feb 27	14	48000	ThAr/RECON RV
High resolution radial velocity				
Subaru 8.2 m/HDS	2012 Sep 20–22	9	60000	I <sub>2</sub> /RV <sup>c</sup>
Magellan 6.5 m/PFS	2012 Dec 28–2013 Mar 4	12	76000	I <sub>2</sub> /RV

<sup>a</sup> Reconnaissance observations used for initial spectral classifications

<sup>b</sup> Reconnaissance observations used to constrain the radial velocity variations

<sup>c</sup> High precision radial velocities to determine the spectroscopic orbit of the planet

TABLE 3  
RELATIVE RADIAL VELOCITIES AND BISECTOR SPAN MEASUREMENTS OF HATS-5.

BJD (2 400 000+)	RV <sup>a</sup> (m s <sup>-1</sup> )	$\sigma_{RV}$ <sup>b</sup> (m s <sup>-1</sup> )	BS (m s <sup>-1</sup> )	$\sigma_{BS}$	Phase	Instrument
56190.07247	...	...	-12.2	32.1	0.425	Subaru (I <sub>2</sub> free) <sup>c</sup>
56190.08373	...	...	-15.3	29.4	0.427	Subaru (I <sub>2</sub> free)
56190.09502	...	...	-19.4	31.8	0.429	Subaru (I <sub>2</sub> free)
56191.05697	24.85	6.66	12.1	29.7	0.631	Subaru
56191.07042	18.93	7.04	18.7	30.8	0.634	Subaru
56191.08294	24.24	5.97	-14.8	31.7	0.637	Subaru
56192.05128	23.95	5.36	10.3	30.5	0.840	Subaru
56192.06253	25.71	5.57	-0.7	30.2	0.842	Subaru
56192.07379	18.94	6.40	18.5	25.1	0.845	Subaru
56193.04260	2.96	6.68	-20.6	32.5	0.048	Subaru
56193.05386	-6.50	6.59	-1.5	26.4	0.051	Subaru
56193.06522	-11.85	5.82	-4.7	31.1	0.053	Subaru
56289.54439	-31.21	3.04	...	...	0.307	PFS
56289.55987	-27.51	3.19	...	...	0.311	PFS
56290.68128	5.01	2.26	...	...	0.546	PFS
56290.69567	11.78	2.39	...	...	0.549	PFS
56291.70608	26.14	2.45	...	...	0.761	PFS
56291.72039	35.20	2.67	...	...	0.764	PFS
56292.65654	5.09	2.78	...	...	0.961	PFS
56292.67135	12.18	2.99	...	...	0.964	PFS
56344.52893	20.99	2.92	...	...	0.850	PFS
56344.54311	26.12	2.91	...	...	0.853	PFS
56355.51803	-28.79	3.80	...	...	0.157	PFS
56355.53239	-19.60	4.73	...	...	0.160	PFS

<sup>a</sup> An instrumental offset in the velocities ( $\gamma_{rel}$ ) from each instrument was fitted for and subtracted in the analysis and the values presented in this table. Observations without an RV measurement are I<sub>2</sub>-free template observations, for which only the bisector (BS) is measured.

<sup>b</sup> Internal errors excluding the component of astrophysical/instrumental jitter considered in Section 3.

<sup>c</sup> HDS template observations made without the Iodine cell. We only measure the BS values for these observations.

in Table 5, the fitted system parameters and derived planet properties in Table 6.

To rule out the possibility that HATS-5 is a blended eclipsing stellar binary system, rather than a transiting planet system, we carried out a blend analysis following Hartman et al. (2011). Based on the light curves, spectroscopically determined atmospheric parameters, and absolute photometry, we are able to exclude scenarios involving a stellar binary blended with a third star (either physically associated, or not associated with the binary) with  $7\sigma$  confidence. In order to fit the light curves, the blend scenarios require a combination of stars with redder broad-band colours than are observed. Moreover,

the best-fit blend model would produce RV variations of several km s<sup>-1</sup> and bisector variations of several hundred m s<sup>-1</sup>, which are substantially greater than the observed variations. We conclude that the observations of HATS-5 are best explained by a model consisting of a planet transiting a star.

To search for rotational modulations of the host star, we perform a Lomb-Scargle (Lomb 1976; Scargle 1982) analysis of the HATSouth discovery light curves, with the transits masked. No statistically significant peaks were identified in the TFA light curves. The expected rotation period from the spectroscopic  $v \sin i$  measurement is 34 days, which is difficult to measure from ground-based

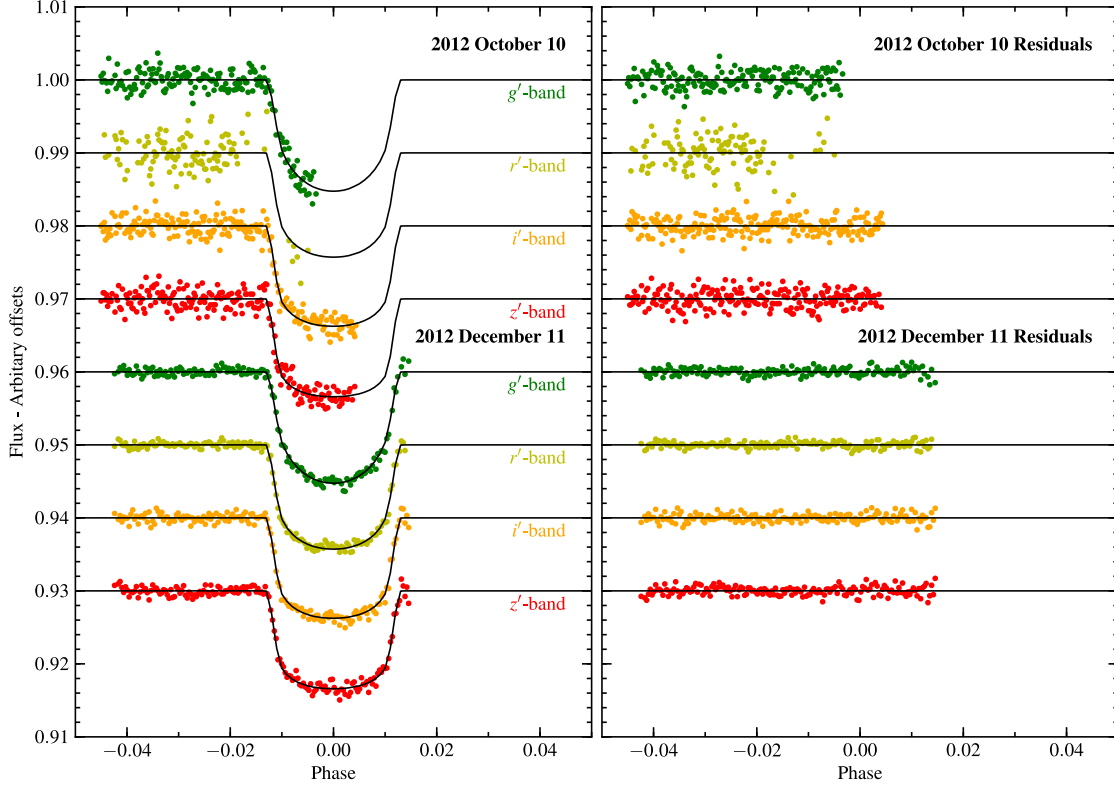


FIG. 3.— *Left*: GROND follow-up transit light curves in the  $g'$ -,  $r'$ -,  $i'$ - and  $z'$ -band are plotted. The light curves have been treated with EPD simultaneous to the transit fitting (Section 3). The best fit model is plotted as a solid line for each observation. *Right*: Residuals for each transit observation is plotted.

TABLE 4  
DIFFERENTIAL PHOTOMETRY OF HATS-5

BJD (2 400 000+)	Mag <sup>a</sup>	$\sigma_{\text{Mag}}$	Mag(orig) <sup>b</sup>	Filter	Instrument
55547.37447	-0.01041	0.00339	...	$r$	HS
55456.87046	0.00039	0.00321	...	$r$	HS
55485.45085	-0.00200	0.00337	...	$r$	HS
55518.79459	-0.00569	0.00345	...	$r$	HS
55499.74154	-0.00095	0.00326	...	$r$	HS
55461.63555	-0.00360	0.00332	...	$r$	HS
55547.37789	0.00305	0.00349	...	$r$	HS
55456.87378	0.00536	0.00324	...	$r$	HS
55518.79794	-0.00583	0.00346	...	$r$	HS
55499.74522	0.00102	0.00328	...	$r$	HS

NOTE. — This table is available in a machine-readable form in the online journal. A portion is shown here for guidance regarding its form and content.

<sup>a</sup> Magnitudes have the out-of-transit level subtracted. HATSouth magnitudes (HS) have been treated with EPD and TFA prior to the transit fitting. The detrending and potential blending may cause the HATSouth transit to be up to 8% shallower than the true transit. Follow-up light curves from GROND have been treated with EPD simultaneous to the transit fitting.

<sup>b</sup> Pre-EPD magnitudes are presented for the follow-up light curves.

photometry (most of the HATSouth photometric data for HATS-5b were gathered over  $\sim 3$  months). We find no emission features in the Calcium H and K lines in the iodine free HDS and PFS spectra, indicating minimal chromospheric activity. The slow rotation rate and the lack of chromospheric activity are both consistent with the isochrone age estimate for HATS-5.

### 3.1. Constraining the radius–wavelength dependency of HATS-5b

Multi-band transit observations by GROND can provide constraints on the dependency between planet radius and wavelength (e.g. Nikolov et al. 2013; Mancini et al. 2013), and potentially probe for molecular absorption and Rayleigh scattering features in the transmission spectrum of a planet. We performed a separate fitting of the GROND full transit data from

TABLE 5  
STELLAR PARAMETERS FOR HATS-5

Parameter	Value	Source
Catalogue Information		
GSC .....	5897-00933	
2MASS .....	04285348-2128548	
RA (J2000) .....	04 <sup>h</sup> 28 <sup>m</sup> 53.47 <sup>s</sup>	2MASS
DEC (J2000) .....	−21°28′54.9″	2MASS
Spectroscopic properties		
$T_{\text{eff}\star}$ (K) .....	$5304 \pm 50$	SPC <sup>a</sup>
[Fe/H] .....	$0.19 \pm 0.08$	SPC
$v \sin i$ (km s <sup>−1</sup> ) .....	$0.8 \pm 0.5$	SPC
Photometric properties		
$V$ (mag) .....	$12.630 \pm 0.030$	APASS
$B$ (mag) .....	$13.439 \pm 0.010$	APASS
$J$ (mag) .....	$11.199 \pm 0.023$	2MASS
$H$ (mag) .....	$10.772 \pm 0.023$	2MASS
$K_s$ (mag) .....	$10.703 \pm 0.023$	2MASS
Derived properties		
$M_\star$ ( $M_\odot$ ) .....	$0.936 \pm 0.028$	YY+ $a/R_\star$ +SPC <sup>b</sup>
$R_\star$ ( $R_\odot$ ) .....	$0.871 \pm 0.023$	YY+ $a/R_\star$ +SPC
$\log g_\star$ (cgs) .....	$4.53 \pm 0.02$	YY+ $a/R_\star$ +SPC
$L_\star$ ( $L_\odot$ ) .....	$0.54 \pm 0.04$	YY+ $a/R_\star$ +SPC
$M_V$ (mag) .....	$5.60 \pm 0.09$	YY+ $a/R_\star$ +SPC
$M_K$ (mag, ESO) ..	$3.69 \pm 0.06$	YY+ $a/R_\star$ +SPC
Age (Gyr) .....	$3.6^{+2.6}_{-1.9}$	YY+ $a/R_\star$ +SPC
Distance (pc) .....	$257 \pm 8$	YY+ $a/R_\star$ +SPC

<sup>a</sup> SPC: The stellar parameters are derived from the PFS iodine-free spectrum using the Stellar Parameter Classification (SPC) pipeline (Buchhave et al. 2012). These parameters also have small dependences on the global model fit and isochrone search iterations.

<sup>b</sup> YY+ $a/R_\star$ +SPC: Based on the YY isochrones (Yi et al. 2001),  $a/R_\star$  as a luminosity indicator, and the SPC results.

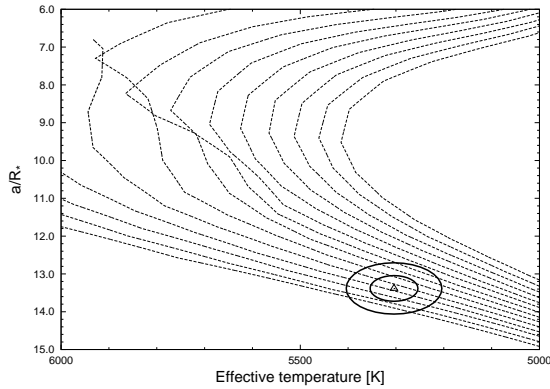


FIG. 4.— Model isochrones from Yi et al. (2001) for HATS-5 are plotted. The isochrones for [Fe/H] = +0.19, ages of 0.2 Gyr (lowest dashed line), and 1 to 13 Gyr in 1 Gyr increments are shown from left to right. The SPC values for  $T_{\text{eff}\star}$  and  $a/R_\star$  are marked by the open triangle, the  $1\sigma$  and  $2\sigma$  confidence ellipsoids are marked by solid lines.

2012 December 11, simultaneously fitting for the transit parameters  $T_c$ ,  $a/R_\star$ , and  $i$ , and the individual  $R_p/R_\star$  for each passband. The fitting is performed using the JKTEBOP eclipsing binary model (Nelson & Davis 1972; Southworth et al. 2004), with both quadratic limb darkening coefficients fixed to that of Claret (2004), and freed and parameterised according to Kipping (2013). The best fit parameters and uncertainties are explored by the *emcee* implementation of a Markov chain Monte Carlo routine (Foreman-Mackey et al. 2012) under Python. Simultaneous EPD is performed on the resid-

uals for each iteration with a linear combination of the first order terms for time, target star X position, Y position, full width at half maximum, and airmass. The final  $R_p/R_\star$  values are consistent with each other to within errors for the fixed and free limb darkening coefficient analyses.

The deviation from mean radius for each passband is plotted in Figure 5. For comparison, we also plot the wavelength-radius variation of HD 189733b, as measured using the Hubble Space Telescope (HST) by Pont et al. (2008); Sing et al. (2011), and scaled to match the scale height (500 km) and  $R_p/R_\star$  of HATS-5b, assuming an H<sub>2</sub> dominated atmosphere (following Snellen et al. 2008). HD 189733b is a pL class planet according to Fortney et al. (2008), with a mildly irradiated atmosphere that is potentially similar to that of HATS-5b. The results of the GROND observations are consistent with both a null detection of atmospheric features and that expected from the scaled measurements of HD 189733b. We do not see obvious star spot crossing events in the transit light curve, although unocculted spots can also cause a slope in the broadband  $R_p/R_\star$  measurements (e.g. Pont et al. 2008; Sing et al. 2011). Whilst we do not detect any atmospheric features on HATS-5b, the large scale height makes HATS-5b an appealing target for future transmission spectroscopy observations. Future observations in the bluer  $U$ -band may also reveal opacity variations in the atmosphere by H<sub>2</sub> Rayleigh scattering (e.g. Sing et al. 2011, 2013; Jordán et al. 2013; Nascimbeni et al. 2013).

TABLE 6  
ORBITAL AND PLANETARY PARAMETERS

Parameter	Value
Light curve parameters	
$P$ (days) .....	$4.763387 \pm 0.000010$
$T_c$ (BJD) <sup>a</sup> .....	$2456273.79068 \pm 0.00010$
$T_{14}$ (days) <sup>a</sup> .....	$0.1244 \pm 0.0004$
$T_{12} = T_{34}$ (days) <sup>a</sup> .....	$0.0124 \pm 0.0003$
$a/R_*$ .....	$13.38 \pm 0.34$
$\zeta/R_*$ <sup>b</sup> .....	$17.85 \pm 0.03$
$R_p/R_*$ .....	$0.1076 \pm 0.0004$
$b \equiv a \cos i/R_*$ .....	$0.158^{+0.057}_{-0.064}$
$i$ (deg) .....	$89.3 \pm 0.3$
Limb-darkening coefficients <sup>c</sup>	
$a_r$ (linear term) .....	0.4723
$b_r$ (quadratic term) .....	0.2542
$a_R$ .....	0.4405
$b_R$ .....	0.2628
$a_i$ .....	0.3571
$b_i$ .....	0.2823
RV parameters	
$K$ (m s <sup>-1</sup> ) .....	$30.0 \pm 1.4$
$\sqrt{e} \cos \omega$ .....	$0.017 \pm 0.090$
$\sqrt{e} \sin \omega$ .....	$-0.015 \pm 0.121$
$e \cos \omega$ .....	$0.001 \pm 0.016$
$e \sin \omega$ .....	$-0.001 \pm 0.024$
$e$ .....	$0.019 \pm 0.019$
$\omega$ .....	$204 \pm 107$
PFS RV jitter (m s <sup>-1</sup> ) <sup>d</sup> .....	2.0
HDS RV jitter (m s <sup>-1</sup> ) .....	0.0
Planetary parameters	
$M_p$ ( $M_J$ ) .....	$0.237 \pm 0.012$
$R_p$ ( $R_J$ ) .....	$0.912 \pm 0.025$
$C(M_p, R_p)$ <sup>e</sup> .....	-0.01
$\rho_p$ (g cm <sup>-3</sup> ) .....	$0.39 \pm 0.04$
$\log g_p$ (cgs) .....	$2.85 \pm 0.03$
$a$ (AU) .....	$0.0542 \pm 0.0006$
$T_{\text{eq}}$ (K) .....	$1025 \pm 17$
$\Theta^f$ .....	$0.030 \pm 0.002$
$\langle F \rangle$ (10 <sup>8</sup> erg s <sup>-1</sup> cm <sup>-2</sup> ) <sup>g</sup> .....	$2.50 \pm 0.17$

<sup>a</sup>  $T_c$ : Reference epoch of mid transit that minimizes the correlation with the orbital period. BJD is calculated from UTC.  $T_{14}$ : total transit duration, time between first to last contact;  $T_{12} = T_{34}$ : ingress/egress time, time between first and second, or third and fourth contact.

<sup>b</sup> Reciprocal of the half duration of the transit used as a jump parameter in our MCMC analysis in place of  $a/R_*$ . It is related to  $a/R_*$  by the expression  $\zeta/R_* = a/R_*(2\pi(1 + e \sin \omega))/(P\sqrt{1 - b^2}\sqrt{1 - e^2})$  (Bakos et al. 2010).

<sup>c</sup> Values for a quadratic law given separately for the Sloan  $g$ ,  $r$ , and  $i$  filters. These values were adopted from the tabulations by Claret (2004) according to the spectroscopic (SPC) parameters listed in Table 5.

<sup>d</sup> This jitter was added in quadrature to the RV uncertainties for each instrument such that  $\chi^2/\text{dof} = 1$  for the observations from that instrument. In the case of HDS,  $\chi^2/\text{dof} < 1$ , so no jitter was added.

<sup>e</sup> Correlation coefficient between the planetary mass  $M_p$  and radius  $R_p$ .

<sup>f</sup> The Safronov number is given by  $\Theta = \frac{1}{2}(V_{\text{esc}}/V_{\text{orb}})^2 = (a/R_p)(M_p/M_*)$  (see Hansen & Barman 2007).

<sup>g</sup> Incoming flux per unit surface area, averaged over the orbit.

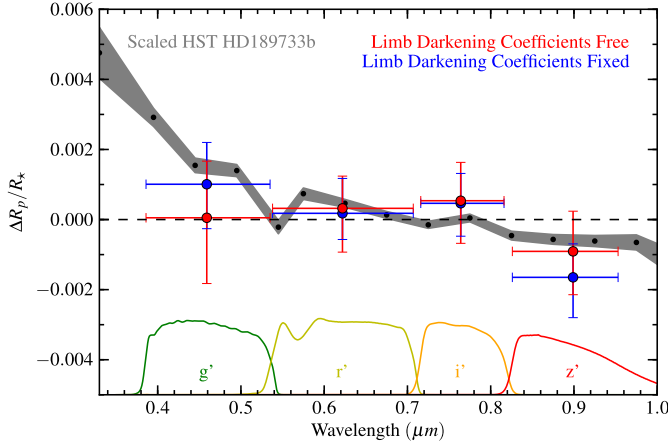


FIG. 5.— Variations in  $R_p/R_*$  over the optical passbands for the GROND full transit on 2012 December 11. A mean radius ratio has been subtracted for each passband. The radius ratios from the limb darkening fixed (blue) and free (red) analyses are plotted. We also plot the transmission spectrum of HD 189733b as observed using HST by Pont et al. (2008); Sing et al. (2011), and scaled to match the scale height and radius ratio of HATS-5b. The transmission curves for each filter are plotted at the bottom.

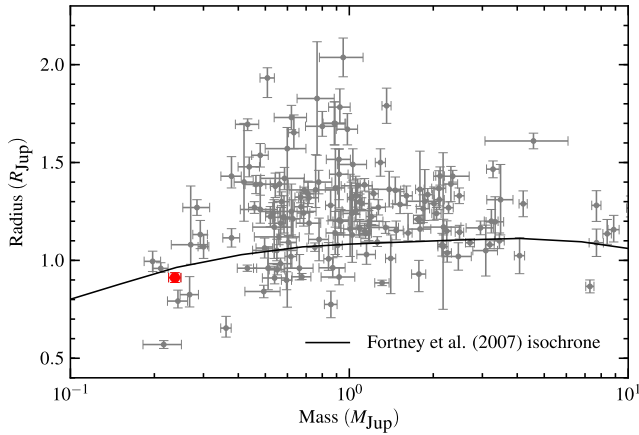


FIG. 6.— The mass-radius distribution of transiting gas giants<sup>a</sup> ( $M_p > 0.1 M_J$ ,  $P < 10$  d) are plotted. HATS-5b is marked in red. Confirmed planets with masses and radii are plotted in gray. The isochrone from Fortney et al. (2007) for 4.5 Gyr old gas-giant planets, with  $10 M_{\text{Earth}}$  core sizes, orbiting 0.045 AU from the host star, is shown by solid line.

<sup>a</sup>As of 12 Dec 2013, [exoplanets.org](http://exoplanets.org)

#### 4. DISCUSSION

We presented the discovery of HATS-5b, a transiting hot-Saturn with mass of  $0.237 \pm 0.012 M_J$  and radius of  $0.912 \pm 0.025 R_J$ . HATS-5b is the the lowest mass and radius planet to date reported by the HATSouth survey. The host star is a quiet, slowly rotating G-dwarf with a stellar mass of  $0.936 \pm 0.028 M_\odot$  and radius of  $0.871 \pm 0.023 R_\odot$ . The mass and radius of HATS-5b are plotted in the context of existing close-in transiting gas giants in Figure 6.

The radius of HATS-5b is consistent with the model of an irradiated gas-giant that formed via core accretion (Fortney et al. 2007). The radius is also consistent within  $1\sigma$  to the empirical radius relationship for Saturn-mass planets from Enoch et al. (2012). We examine below the empirical factors that affect the radius of irradi-

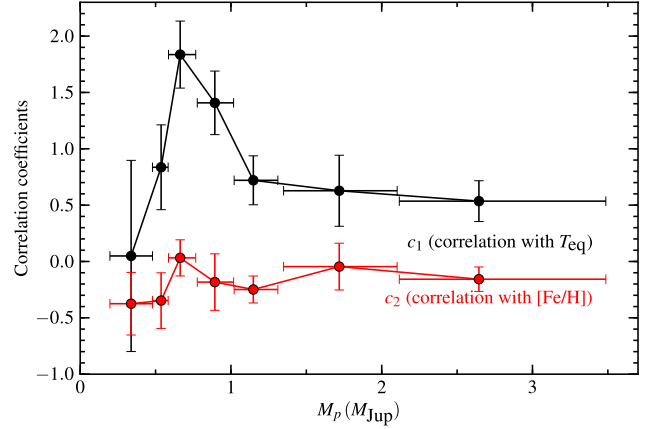


FIG. 7.— The correlation between planet radius, equilibrium temperature and metallicity are plotted. For each mass bin of size 20, we calculate the correlation coefficients  $c_1$  and  $c_2$  (Equation 1). The vertical error bars are derived from bootstrapping the sample. The horizontal error bars show the extent of each mass bin.

ated gas-giants.

##### 4.1. The $T_{\text{eq}}$ -[Fe/H]-radius relationship

A number of previous studies have investigated the relationship between the planet radius distribution, host star metallicity, and levels of insolation (e.g. Guillot et al. 2006; Enoch et al. 2011; Béky et al. 2011; Enoch et al. 2012). The factors that impact the radius of a gas giant should be mass dependent. For example, the level insolation should have a less significant impact on the radius of the denser, more massive gas giants and brown dwarfs than on the less dense Saturn-mass planets. Here, we revisit the mass dependence of the planet radius on the host star metallicity and the planet equilibrium temperature.

We bin the planet population into samples of 20, and perform a least squares fit for a linear dependence between radius, mass, equilibrium temperature  $T_{\text{eq}}$ , and metallicity:

$$R_{\text{model}} = c_1 \mathcal{T} + c_2 \mathcal{M} + c_3 \log M_p + c_4 \quad (1)$$

$$\mathcal{T} \equiv \frac{T_{\text{eq}} - T_{\text{eq,mean}}}{T_{\text{eq,max}} - T_{\text{eq,min}}}$$

$$\mathcal{M} \equiv \frac{[\text{Fe}/\text{H}] - [\text{Fe}/\text{H}]_{\text{mean}}}{[\text{Fe}/\text{H}]_{\text{max}} - [\text{Fe}/\text{H}]_{\text{min}}}$$

where the magnitude of  $c_1$  and  $c_2$  are used to judge the level of correlation for  $T_{\text{eq}}$  and [Fe/H], respectively.  $c_3$  takes into account a linear dependence between mass and radius within the mass bin.  $c_4$  is an arbitrary offset in the fit. The errors in the coefficients are derived by bootstrapping the analysis within each mass bin. Since each mass bin covers a relatively small mass range, a linear dependence is sufficient (see Figure 7 for the sizes of each mass bin). We find a peak in the mass dependence of the  $T_{\text{eq}}$  correlation at  $M_p \sim 1 M_J$ , and a general lack of overall correlation between  $R_p$  and [Fe/H]. The correlation coefficients are plotted against their respective mass bins in Figure 7. We repeated the exercise using only planets with solar-mass hosts ( $0.8 < M_\star < 1.2 M_\odot$ ), to reduce any potential selection effects in the target selection and spectral classifications



of the surveys. Smaller planets are found in longer periods (e.g. Mazeh et al. 2005; Davis & Wheatley 2009), biasing the  $T_{\text{eq}}$ -mass distribution. To reduce the effect of the bias, we re-perform the analysis using only mildly irradiated planets ( $T_{\text{eq}} < 1500$  K). In addition, the radius- $T_{\text{eq}}$  dependence is non-linear over the general population (Demory & Seager 2011), limiting the  $T_{\text{eq}}$  range has the added benefit of reducing effect of the non-linear dependence on the analysis. In all cases we find the peak dependence to  $T_{\text{eq}}$  to be  $\sim 1 M_J$ , and a lack of dependence on  $[\text{Fe}/\text{H}]$ .

We also perform the same analysis for the entire population of hot gas-giants, fitting for a second order polynomial in mass-radius, and linear dependence to  $T_{\text{eq}}$  and  $[\text{Fe}/\text{H}]$ . We find a strong correlation in  $T_{\text{eq}}$  with  $c_1 = 0.81 \pm 0.17$ , and an insignificant correlation in  $[\text{Fe}/\text{H}]$ , with  $c_2 = -0.25 \pm 0.14$ . Increasing the order of the polynomial does not affect the coefficient values within errors. We find the overall dependence to  $[\text{Fe}/\text{H}]$  to be weak at best. Miller & Fortney (2011) suggests that the  $[\text{Fe}/\text{H}]$ -radius dependence is more prominent for the least irradiated planets, we limit the analysis to planets with  $T_{\text{eq}} < 1500$  K, but still find a lack of correlation with  $[\text{Fe}/\text{H}]$ , with  $c_1 = 0.37 \pm 0.11$  and  $c_2 = -0.15 \pm 0.10$ .

We find the radius of Saturn-mass planets are less affected by their equilibrium temperature than Jupiter-mass planets, in agreement with the Singular Value Decomposition analysis performed by Enoch et al. (2012). In addition, we also find that the radius of planets with  $M_p > 1 M_J$  are also less dependent on equilibrium temperature. This effect is reproduced by the isochrones from Fortney et al. (2007). The isochrones can also reproduce a drop in the correlation strength between irradiation and radius for the least massive gas-giants ( $M_p < 0.3 M_J$ ), but require the presence of a large core ( $M_c > 10 M_{\text{Earth}}$ ). Interestingly, we find no statistically significant dependence of radius on the host star metallicity, contrary to previous examinations (e.g. Guillot et al. 2006; Béky et al. 2011; Enoch et al. 2011, 2012). It is not clear how the host star metallicity affects the metallicity and radius of the planet. A higher metallicity disk may produce planets with more massive cores, leading to a smaller overall radius (e.g. Guillot et al. 2006), but a higher opacity atmosphere is more efficient at retaining

heat, reducing the rate of contraction, leading to a more inflated radius (e.g. Burrows et al. 2007, 2011).

Development of the HATSouth project was funded by NSF MRI grant NSF/AST-0723074, operations are supported by NASA grant NNX12AH91H, and follow-up observations receive partial support from grant NSF/AST-1108686. Work at the Australian National University is supported by ARC Laureate Fellowship Grant FL0992131. Followup observations with the ESO 2.2m/FEROS instrument were performed under MPI guaranteed time (P087.A-9014(A), P088.A-9008(A), P089.A-9008(A)) and Chilean time (P087.C-0508(A)). A.J. acknowledges support from FONDECYT project 1130857, BASAL CATA PFB-06, and the Millennium Science Initiative, Chilean Ministry of Economy (Millennium Institute of Astrophysics MAS and Nucleus P10-022-F). V.S. acknowledges support from BASAL CATA PFB-06. M.R. acknowledges support from FONDECYT postdoctoral fellowship No3120097. R.B. and N.E. acknowledge support from CONICYT-PCHA/Doctorado Nacional and Fondecyt project 1130857. This work is based on observations made with ESO Telescopes at the La Silla Observatory under programme IDs P087.A-9014(A), P088.A-9008(A), P089.A-9008(A), P087.C-0508(A), P089.A-9006(A), and We acknowledge the use of the AAVSO Photometric All-Sky Survey (APASS), funded by the Robert Martin Ayers Sciences Fund, and the SIMBAD database, operated at CDS, Strasbourg, France. Operations at the MPG/ESO 2.2m Telescope are jointly performed by the Max Planck Gesellschaft and the European Southern Observatory. The imaging system GROND has been built by the high-energy group of MPE in collaboration with the LSW Tautenburg and ESO. We thank Rgis Lachaume for his technical assistance during the observations at the MPG/ESO 2.2m Telescope. Australian access to the Magellan Telescopes was supported through the National Collaborative Research Infrastructure Strategy of the Australian Federal Government. We thank Albert Jahnke, Toni Hanke (HESS), Peter Conroy (MSO) for their contributions to the HATSouth project.

## REFERENCES

- Bakos, G., Noyes, R. W., Kovács, G., et al. 2004, *PASP*, 116, 266  
 Bakos, G. Á., Kovács, G., Torres, G., et al. 2007, *ApJ*, 670, 826  
 Bakos, G. Á., Torres, G., Pál, A., et al. 2010, *ApJ*, 710, 1724  
 Bakos, G. Á., Csabry, Z., Penev, K., et al. 2013, *PASP*, 125, 154  
 Bayliss, D., Zhou, G., Penev, K., et al. 2013, *AJ*, 146, 113  
 Béky, B., Bakos, G. Á., Hartman, J., et al. 2011, *ApJ*, 734, 109  
 Borucki, W. J., Koch, D., Basri, G., et al. 2010, *Science*, 327, 977  
 Buchhave, L. A., Latham, D. W., Johansen, A., et al. 2012, *Nature*, 486, 375  
 Burrows, A., Heng, K., & Nampaisarn, T. 2011, *ApJ*, 736, 47  
 Burrows, A., Hubeny, I., Budaj, J., & Hubbard, W. B. 2007, *ApJ*, 661, 502  
 Butler, R. P., Marcy, G. W., Williams, E., et al. 1996, *PASP*, 108, 500  
 Charbonneau, D., Brown, T. M., Noyes, R. W., & Gilliland, R. L. 2002, *ApJ*, 568, 377  
 Claret, A. 2004, *A&A*, 428, 1001  
 Cowan, N. B., & Agol, E. 2011, *ApJ*, 729, 54  
 Crane, J. D., Shtetman, S. A., Butler, R. P., et al. 2010, in *Society of Photo-Optical Instrumentation Engineers (SPIE) Conference Series*, Vol. 7735, Society of Photo-Optical Instrumentation Engineers (SPIE) Conference Series  
 Davis, T. A., & Wheatley, P. J. 2009, *MNRAS*, 396, 1012  
 Deming, D., Seager, S., Richardson, L. J., & Harrington, J. 2005, *Nature*, 434, 740  
 Demory, B.-O., & Seager, S. 2011, *ApJS*, 197, 12  
 Dopita, M., Hart, J., McGregor, P., et al. 2007, *Ap&SS*, 310, 255  
 Enoch, B., Collier Cameron, A., & Horne, K. 2012, *A&A*, 540, A99  
 Enoch, B., Cameron, A. C., Anderson, D. R., et al. 2011, *MNRAS*, 410, 1631  
 Foreman-Mackey, D., Hogg, D. W., Lang, D., & Goodman, J. 2012, *ArXiv e-prints*, 1202.3665  
 Fortney, J. J., Lodders, K., Marley, M. S., & Freedman, R. S. 2008, *ApJ*, 678, 1419  
 Fortney, J. J., Marley, M. S., & Barnes, J. W. 2007, *ApJ*, 659, 1661  
 Fressin, F., Torres, G., Charbonneau, D., et al. 2013, *ApJ*, 766, 81

- Greiner, J., Bornemann, W., Clemens, C., et al. 2008, *PASP*, 120, 405
- Guillot, T., Santos, N. C., Pont, F., et al. 2006, *A&A*, 453, L21
- Hansen, B. M. S., & Barman, T. 2007, *ApJ*, 671, 861
- Hartman, J. D., Bakos, G. Á., Torres, G., et al. 2011, *ApJ*, 742, 59
- Howard, A. W., Marcy, G. W., Bryson, S. T., et al. 2012, *ApJS*, 201, 15
- Jordán, A., Espinoza, N., Rabus, M., et al. 2013, *ApJ*, 778, 184
- Kambe, E., Sato, B., Takeda, Y., et al. 2002, *PASJ*, 54, 865
- Kipping, D. M. 2013, *MNRAS*, 435, 2152
- Kovács, G., Bakos, G., & Noyes, R. W. 2005, *MNRAS*, 356, 557
- Kovács, G., Zucker, S., & Mazeh, T. 2002, *A&A*, 391, 369
- Lomb, N. R. 1976, *Ap&SS*, 39, 447
- Mancini, L., Ciceri, S., Chen, G., et al. 2013, *MNRAS*, 436, 2
- Mazeh, T., Zucker, S., & Pont, F. 2005, *MNRAS*, 356, 955
- Miller, N., & Fortney, J. J. 2011, *ApJ*, 736, L29
- Mohler-Fischer, M., Mancini, L., Hartman, J. D., et al. 2013, *A&A*, 558, A55
- Nascimbeni, V., Piotto, G., Pagano, I., et al. 2013, *A&A*, 559, A32
- Nelson, B., & Davis, W. D. 1972, *ApJ*, 174, 617
- Nikolov, N., Chen, G., Fortney, J. J., et al. 2013, *A&A*, 553, A26
- Noguchi, K., Aoki, W., Kawanomoto, S., et al. 2002, *PASJ*, 54, 855
- Penev, K., Bakos, G. Á., Bayliss, D., et al. 2013, *AJ*, 145, 5
- Pollacco, D. L., Skillen, I., Collier Cameron, A., et al. 2006, *PASP*, 118, 1407
- Pont, F., Knutson, H., Gilliland, R. L., Moutou, C., & Charbonneau, D. 2008, *MNRAS*, 385, 109
- Queloz, D., Eggenberger, A., Mayor, M., et al. 2000, *A&A*, 359, L13
- Santos, N. C., Israelian, G., & Mayor, M. 2004, *A&A*, 415, 1153
- Sato, B., Kambe, E., Takeda, Y., Izumiura, H., & Ando, H. 2002, *PASJ*, 54, 873
- Sato, B., Hartman, J. D., Bakos, G. Á., et al. 2012, *PASJ*, 64, 97
- Scargle, J. D. 1982, *ApJ*, 263, 835
- Sing, D. K., Pont, F., Aigrain, S., et al. 2011, *MNRAS*, 416, 1443
- Sing, D. K., Lecavelier des Etangs, A., Fortney, J. J., et al. 2013, *MNRAS*, 436, 2956
- Snellen, I. A. G., Albrecht, S., de Mooij, E. J. W., & Le Poole, R. S. 2008, *A&A*, 487, 357
- Southworth, J., Maxted, P. F. L., & Smalley, B. 2004, *MNRAS*, 351, 1277
- Sozzetti, A., Torres, G., Charbonneau, D., et al. 2007, *ApJ*, 664, 1190
- Yi, S., Demarque, P., Kim, Y.-C., et al. 2001, *ApJS*, 136, 417
- Zhou, G., Bayliss, D., Hartman, J. D., et al. 2013, *ArXiv e-prints*, 1310.7591